ACS APPLIED MATERIALS & INTERFACES

Research Article

www.acsami.org

Engineered High Aspect Ratio Vertical Nanotubes as a Model System for the Investigation of Catalytic Methanol Synthesis Over Cu/ZnO

Firat Güder,*[,†] Elias Frei,*[,‡] Umut M. Kücükbayrak,[†] Andreas Menzel,[†] Ralf Thomann,[§] Roman Luptak,[∥,⊥] Bernd Hollaender,[∥] Ingo Krossing,[‡] and Margit Zacharias[†]

[†]Laboratory for Nanotechnology, Department of Microsystems Engineering (IMTEK), University of Freiburg, Freiburg 79110, Germany

[‡]Institute for Inorganic and Organic Chemistry, University of Freiburg, Freiburg 79104, Germany

[§]Freiburger Material Forschungszentrum (FMF), University of Freiburg, Freiburg 79104, Germany

[∥]Forschungszentrum Juelich GmbH, Juelich 52425, Germany

Supporting Information

ABSTRACT: Catalytically synthesized methanol from H_2 and CO_2 using porous Cu/ZnO aggregates is a promising, carbon neutral, and renewable alternative to replace fossil fuel based transport fuels. However, the absence of surface-engineered model systems to understand and improve the industrial Cu/ZnO catalyst poses a big technological gap in efforts to increase industrial methanol conversion efficiency. In this work, we report a novel process for the fabrication of patterned, vertically aligned high aspect ratio 1D nanostructures on Si that can be used as an engineered model catalyst. The proposed strategy employs near-field phase shift lithography (NF-PSL), deep reactive ion etching (DRIE), and atomic layer deposition (ALD) to pattern, etch, and coat Si wafers to produce high aspect ratio 1D nanostructures. Using this method, we produced a model system consisting of high aspect ratio Cu-decorated ZnO nanotubes (NTs) to investigate the morphological effects of ZnO catalyst support in comparison to the planar Cu/ZnO catalyst in terms of the catalytic reactions. The engineered catalysts performed 70 times better in activating CO_2 than the industrial catalyst. In light of the obtained results, several important points are highlighted, and recommendations are made to achieve higher catalytic performance.

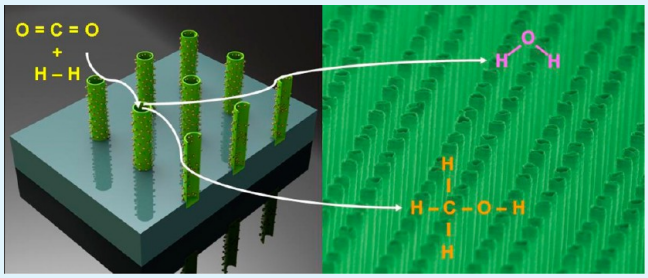

KEYWORDS: *nanotubes, catalysis, atomic layer deposition, phase shift lithography methanol, Cu/ZnO*

Fabrication of vertically oriented metallic, semiconducting, and insulating 1D nanostructures, namely, nanotubes (NTs) and nanowires (NWs), has been the focus of research in several fields of science and technology.[1] Methods to produce precisely positioned NTs and NWs with well-controlled and scalable features such as the diameter, length, and wall thickness are particularly important for the next generation of nanoelectronics, optoelectronics, sensors, drug delivery systems, and many more.[2−5] Aside from being active components in functional devices, NTs and NWs are also valuable structures for the study and investigation of a variety of fundamental phenomena including but not limited to nanoscale void formation, oxidation, strain, stress, deformation, etc.[5−8]

Although there are a multitude of processing techniques that are capable of producing metallic, semiconducting, and insulating vertical NTs and NWs, there is no technology that is able to support high aspect ratio vertical integration of all three kinds of nanowires with accurate spatial positioning on Si. Vertically oriented NTs and NWs are traditionally grown by high-temperature vapor-phase deposition techniques using metal catalysts where the position of the produced structure is defined by the location of the catalyst.[9,10] Template-assisted electrochemical deposition methods have also been used to fabricate vertically oriented 1D nanostructures but have been limited to metals.[11] Top-down approaches using various patterning techniques and micromachining can also be employed for NW/NT fabrication. However, the selection of materials that is suitable for high aspect ratio micromachning is very limited (e.g., Si) and by no means a general strategy for vertically oriented 1D nanostructure fabrication.[9,12]

Increasing CO_2 concentration in the atmosphere, due to use of fossil fuels, is the main human-caused factor behind climate change. According to a report by the United States Environmental Protection Agency (EPA), in 2010 transportation emissions made up 27% of all greenhouse gas emissions, 95% of which was from CO_2.[13] Methanol (CH_3OH), a simple alcohol, offers a renewable and carbon neutral alternative to liquid fossil fuels for transportation. It can be used directly in internal combustion engines and is an effective carrier of hydrogen for fuel cell powered vehicles. Methanol can be

Received: September 30, 2013
Accepted: January 6, 2014
Published: January 6, 2014

   dx.doi.org/10.1021/am4042959 | ACS Appl. Mater. Interfaces 2014, 6, 1576−1582

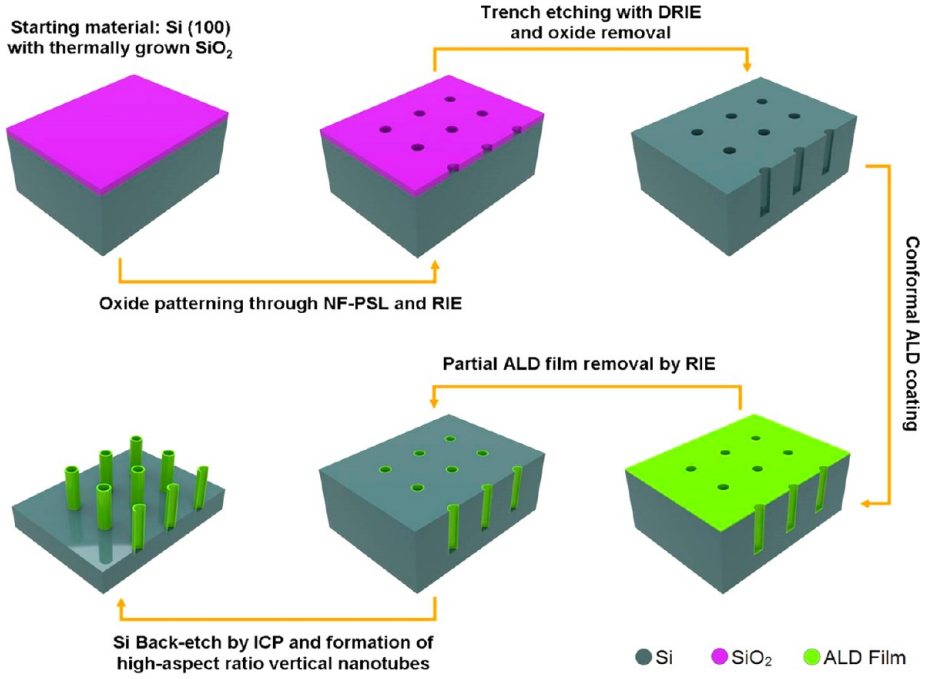

Figure 1. Scheme illustrating the ALD-assisted nanotube/nanowire fabrication process on Si.

produced efficiently by reacting CO_2 and H_2 (eq 1) or CO and H_2 (eq 2) in the presence of a catalyst. The Cu/ZnO industrial catalyst is by far the most commonly used material

$$CO_2 + 3H_2 \rightleftharpoons CH_3OH + H_2O \qquad \Delta H_{298K} = -11.9\ \text{kcal/mol} \tag{1}$$

$$CO + 2H_2 \rightleftharpoons CH_3OH \qquad \Delta H_{298K} = -21.7\ \text{kcal/mol} \tag{2}$$

for the synthesis of methanol with a selectivity reaching up to 99.8%.[14] The commercial Cu/ZnO catalyst is produced by the coprecipitation method, consisting of porous aggregates of Cu and ZnO nanoparticles.[15−17] As these structures are quite dense and complex, studying exactly what is happening with the catalyst system during and after synthesis is not a trivial task. Methanol synthesis over Cu is a structure-sensitive reaction[16] in which ZnO plays the important role of acting as a spacer between the Cu particles and a chemical promoter. Engineered surfaces with well-known and precise properties and geometries can play an important role in mechanism exploration and process optimization in catalytic synthesis with the aim of increasing the efficiency and selectivity of the industrial catalytic systems.

In this report, we propose a versatile fabrication technique, which is capable of producing wafer scale, free-standing, high aspect ratio vertical NTs and NWs on Si. This new strategy is based on atomic layer deposition (ALD), near-field phase shift lithography (NF-PSL), and the well-established Si processing methods. It allows synthesis of metallic, semiconducting, insulating, as well as heterojunction and core−shell 1D nanostuctures of any ALD available material. Using this fabrication regime, we produced vertically oriented, high aspect ratio, Cu-decorated ZnO NT catalysts to study the underlying dynamics of thermocatalytic methanol synthesis with respect to the morphology of the catalyst support.

FABRICATION OF HIGH ASPECT RATIO NANOTUBES AND NANOWIRES

Figure 1 highlights the nanotube/nanowire fabrication process. In the first step, a standard Si(100) wafer with a thermally grown 1 μm SiO_2 layer is coated with photoresist (AZ 5214) and patterned using NF-PSL. More details regarding the patterning process can be found elsewhere.[18,19] The resist pattern was transferred to the oxide layer through reactive ion etching (RIE) with a gas mixture of $CHF_3/CF_4/Ar$. After the pattern transfer, the remaining photoresist was removed in an O_2 plasma asher. In the next step, using deep reactive ion etching (DRIE), also known as the Bosch process, high aspect ratio (HAR) trenches were etched into the Si substrate using C_4F_8 for passivation and SF_6/O_2 for etching. Here, the patterned oxide layer acted as a high selectivity etch mask that permitted deep etching of the underlying Si substrate. Then the oxide is removed from the wafer via a 5% HF dip, and the etched substrate with HAR trenches was coated with an ALD film. Removal of the ALD layer from horizontal surfaces by RIE with only Ar and selective back-etching of Si by inductively coupled plasma (ICP-SF_6/C_4F_8 plasma) etching resulted in HAR NTs and NWs, vertically oriented on Si.

In this fabrication scheme, the two most critical steps were the HAR trench etching with the Bosch process and HAR trench coating by ALD. Both of these process steps were important in defining the final geometry of the produced nanostructures. The Bosch process is a two-step, cyclic plasma etching technique (see SI Figure S1 for more details) that consists of a passivation and an etch step that are repeated sequentially in a plasma system that is equipped with both a coil (for high density plasma generation) and platen plasma generator. In the passivation phase, the Si substrate is coated with a polymer using C_4F_8 (octafluorocyclobutane) plasma. The goal of plasma polymerization is to provide sidewall passivation and increase anisotropy in the etch phase. In a typical etch step, a mixture of SF_6 and O_2 plasma is mixed in varying ratios to first remove the polymer layer from planar

dx.doi.org/10.1021/am4042959 | ACS Appl. Mater. Interfaces 2014, 6, 1576−1582

surfaces and then etch Si from the substrate. A small platen bias is often applied to increase directionality in the etch step and minimize reactions on vertical surfaces. By repeating each process step, HAR trenches with high vertical anisotropy can be etched into Si. However, the cyclic nature of the process causes formation of scalloped vertical sidewalls. Though it is not possible to avoid this phenomenon completely, this effect can be minimized through careful optimization. Figure 2a shows a

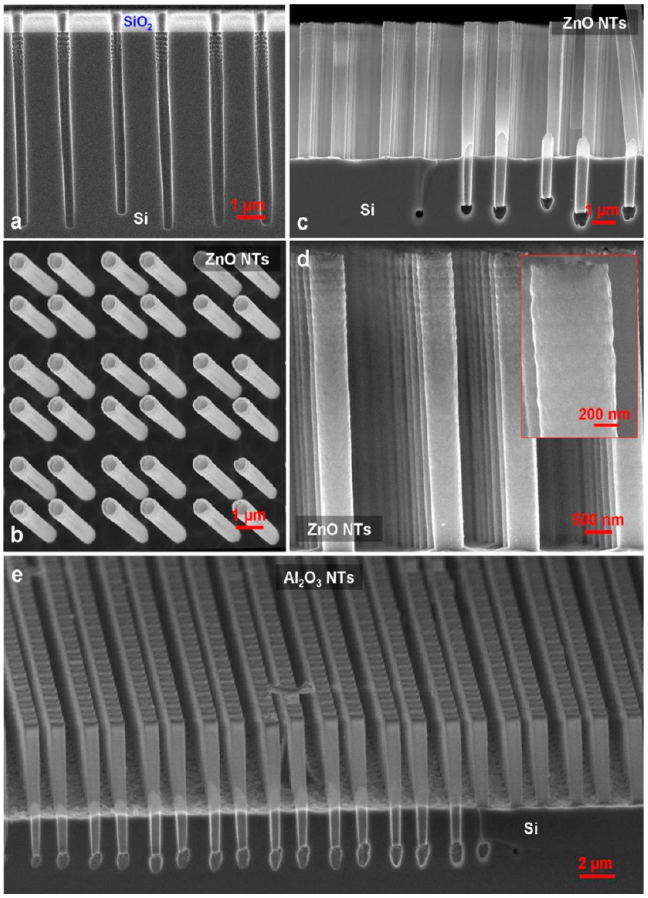

Figure 2. SEM micrographs of (a) cross-sectional view of high aspect ratio Si trenches etched by the Bosch process using the process gasses C_4F_8 for passivation and SF_6/O_2 for etching. Thermal SiO_2 is used as the etch mask. (b) Birds-eye view of an array of ZnO nanotubes produced by the proposed fabrication process. (c) Cross-sectional view of ZnO nanotubes. Nanotubes are partially buried in Si after ICP back-etching. (d) Up-close cross-sectional images of ZnO nanotubes. The inset shows the scalloped surface due to the Bosch process. (e) Wafer scale array of Al_2O_3 nanotubes produced by the same fabrication procedure.

cross-sectional scanning electron microscope (SEM) image of HAR deep trenches etched into Si with an aspect ratio of 10. In this experiment, 85 sccm of SF_6 and 9 sccm of O_2 were used for etching, and 85 sccm of C_4F_8 was used for passivation. An overall Si etch rate of approx. 0.6 μm/min was attained with a coil and platen power of 600 and 25 W, respectively. A step duration of 3 s was set for both, etching and passivation steps, to minimize sidewall scalloping and critical dimension (CD) loss. We have achieved a CD loss of less than 80 nm for the etched Si trenches. Figure S2 (SI) displays SEM images of several trench profiles obtained under different process conditions.

On the other hand, ALD is a sequential chemical vapor deposition (CVD) technique which allows deposition of highly conformal thin films with subnanometer precision on complex 3D structures.[20,21] In ALD, gas-phase precursors are released into the reaction chamber in a cyclic manner, dividing the deposition process into two half surface reactions as opposed to continuous gas reactions of conventional CVD. This property of ALD guarantees deposition of high-quality, pinhole-free conformal thin films in very deep trenches up to an aspect ratio of 10^3.[22] Since the thickness of the deposited films can be controlled with high accuracy, nanotubes with extremely thin walls can be fabricated. The nanotubes can be easily transformed into nanowires by increasing the number of deposition cycles thus the overall film thickness. With a considerable selection of available processes for the deposition of oxides, sulfides, nitride, and elemental thin films, a large variety of NTs and NWs can be synthesized on Si. In recent years, ALD, in combination with porous templates (e.g., anodic alumina) have been applied to fabrication of NTs and NWs to yield 1D nanostructures.[23−25] However, these techniques are not capable of producing vertically oriented 1D nanostructures with precise geometries and positions on Si. As a result, ALD NTs and NWs could not be integrated into Si-based devices, and our proposed method mainly aims at filling this technological gap.

Figure 2b−d shows vertically oriented ZnO HAR nanotubes produced by our ALD-assisted fabrication method. We deposited a 30 nm thick ALD ZnO thin film using diethylzinc and water as precursors at a process temperature of 150 °C. Figure 2b displays a birds-eye-view SEM image of ZnO nanotubes. It can be seen that the NTs are uniformly periodic and depending on the application, the pattern can be modified with NF-PSL. The cross-sectional SEM image of the same ZnO NTs (Figure 2c) highlights the details of the fabricated structures. The image shows that the bottom portions of the NTs are buried inside the Si substrate, securely anchoring them on the surface. This fabrication regime also allows easy adjustment of NT/NW length by reducing and increasing the Si back-etch duration in the final step of fabrication. In fact, NTs and NWs of different lengths can also be produced on the same substrate by masking specific areas during the back-etch process. Figure 2d is an up-close cross-sectional micrograph of the ZnO NTs. The inset clearly shows the formed scallops on the tube walls, which were created by the Bosch process during HAR trench etching. The fabrication method proposed here is a general route for the synthesis of vertical NTs and NWs of various materials. To demonstrate this, we coated another etched Si substrate with 30 nm of ALD Al_2O_3 using the trimethylaluminum/water pair, at again 150 °C. Following the same fabrication procedure resulted in Al_2O_3 NTs (Figure 2e), proving the compatibility of the proposed technique with other ALD materials. Once again, the Al_2O_3 NTs are also partially buried and have the surface scallops as in ZnO NTs, which is characteristic for the overall process.

THERMOCATALYTIC METHANOL SYNTHESIS

Using our engineered surfaces, we investigate the Cu/ZnO thermocatalytic methanol synthesis reaction to determine the effect of catalyst support (ZnO) geometry on the reaction. For this purpose, two samples were prepared. The first sample was planar, 2 × 20 mm in size, and consisted of a 30 nm ALD ZnO thin film deposited on an n-type Si(100) virgin wafer (Figure 3a). The second sample (2 × 10 mm) was prepared with the

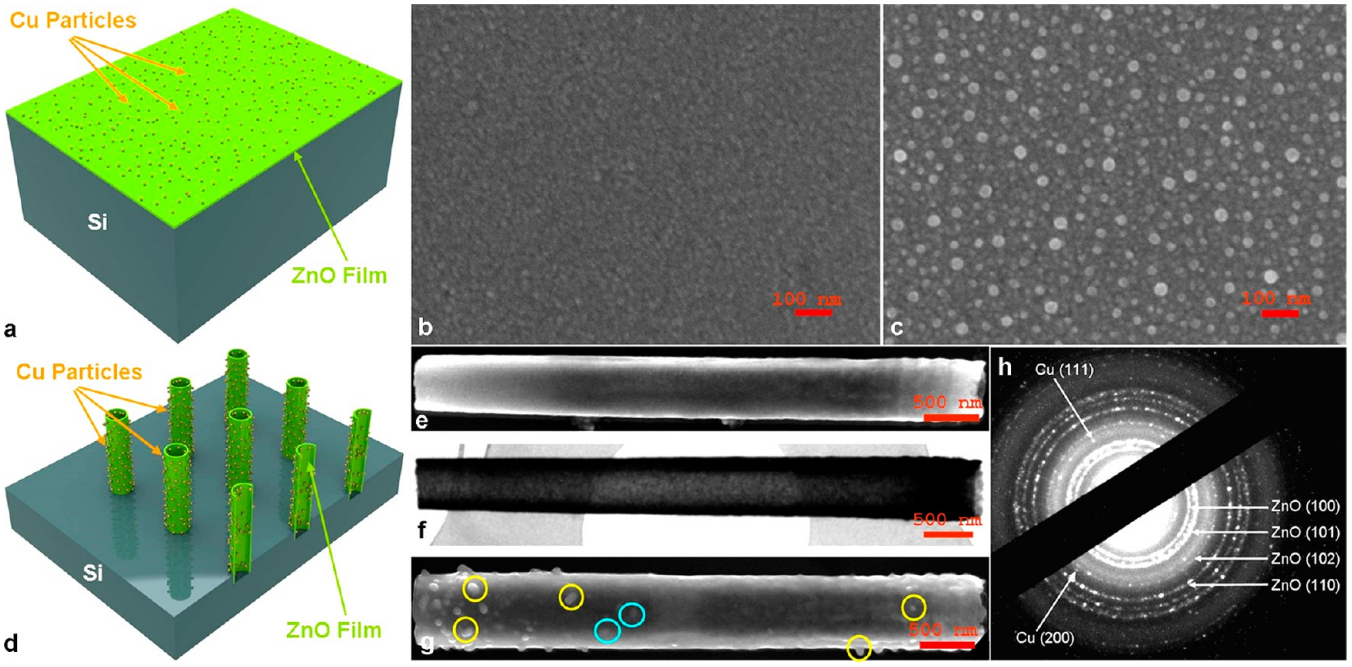

Figure 3. (a) Schematic illustration of the planar Cu/ZnO catalyst. SEM image of the planar Cu/ZnO catalyst surface before (b) and after (c) the methanol synthesis reaction. (d) Schematic illustration of nanotube Cu/ZnO catalyst. (e) SEM and (f) TEM image of a Cu/ZnO nanotube before the reaction. (g) SEM image of a Cu/ZnO nanotube after the reaction. The particles marked with yellow are located on the outer and blue on the inner surface of the tube walls. (h) Electron diffraction data of the nanotube shown in (f).

same 30 nm thick ZnO film and consisted of nanotubes produced with the procedure described previously and shown in Figure 2b–d. Both samples were coated with ~5 nm of Cu (99.99% purity) in a thermal metal evaporator at 5×10^{-5} mbar.

Figure 3b shows the surface of the planar sample before the synthesis reaction. As seen in the figure, the surface is covered with a dense film of Cu particles in the range of 5 nm. However, during the reaction (Figure 3c), these ~5 nm Cu nanoparticles agglomerated into large particles with sizes reaching up to 40–50 nm (i.e., catalyst aging), reducing the total active surface area of Cu and the interface with ZnO. The Cu–ZnO interface is crucial for methanol synthesis. Although we were only partially able to directly observe the Cu nanoparticles on the nanotube surface by SEM (Figure 3e) due to the rough NT surface, we confirmed the existence of Cu by transmission electron microscopy (Figure 3f) and its corresponding electron diffraction pattern (Figure 3h). The diffraction rings originating from ZnO and Cu are clearly visible. We have also performed EDX analysis to investigate the Cu distribution on the nanotubes before the reaction (see SI Figure S3). As seen in the line scan, Cu is not evenly distributed throughout the nanostructure as a result of the technique used to deposit Cu. After the synthesis reaction, SEM observations of the NTs revealed a result similar to the planar sample. Figure 3g shows the surface of an individual NT with agglomerated Cu particles which are mostly concentrated on the top and bottom of the NT. The particles marked with yellow circles are located on the outer NT surface, whereas the blue circles highlight the particles attached to the inner surface of the tube walls. The produced catalysts were tested for 12 h at 220 and 240 °C (each temperature 6 h), 40 bar, and a gas flow of 1600 N mL·h^{-1} with 75% H_2 and 25% CO_2. Figure 4a shows the experimental setup schematically (for more detailed information about the catalyst testing system, see SI Figures S5 and

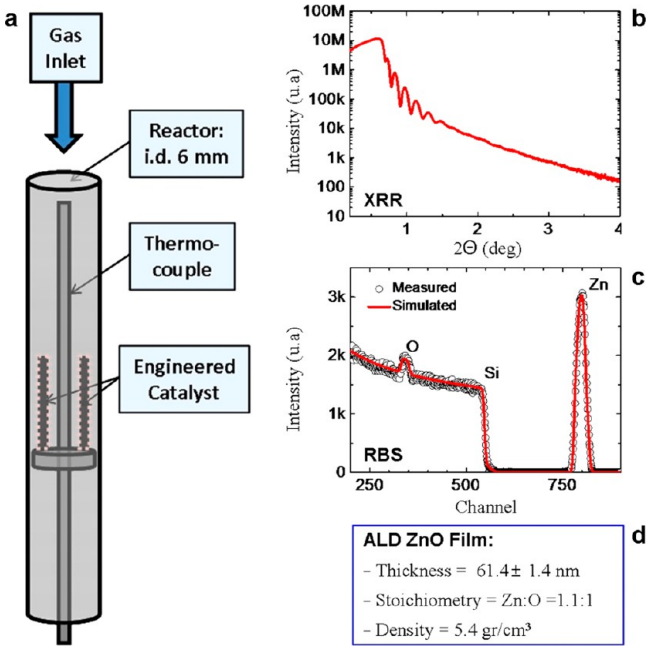

Figure 4. (a) Schematic drawing of the tube reactor (inner diameter 6 mm, stainless steel) and the nanostructured catalyst inside. A three-point thermocouple inside the reactor controls the temperature. The small plate at the thermocouple enabled the fixation of the silicon wafer, coated with Cu/ZnO. Results of (b) XRR and (c) RBS analysis performed on a 60 nm ALD deposited ZnO layer and (d) obtained values for film thickness, stoichiometry, and density.

S6). We performed X-ray reflectivity (Figure 4b) and Rutherford backscattering spectroscopy (RBS) (Figure 4c) analysis on an ALD ZnO film (we doubled film thickness from 30 to 60 nm for more accurate analysis) grown on Si to determine the film density and stoichiometry (Figure 4d).[26]

dx.doi.org/10.1021/am4042959 | ACS Appl. Mater. Interfaces 2014, 6, 1576–1582

Using the obtained film density of 5.4 g/cm^3, we calculated the amount of ZnO on the nanotube and planar samples to be in the range of 0.1 and 0.01 mg, respectively.

Due to the small amount of active catalyst employed (0.01−0.1 mg, cf. classical catalyst loading of 500−1000 mg) and its character as a model system, the GC method was set to a very sensitive mode and operated at a split rate of 10:1, compared to our conventional heterogeneous catalysts setup with a split of 100:1. In general, model systems used in heterogeneous catalysis are not very active, but with an "active" model system all measurements, signals, and surface species are detectable more easily and clearly. The herein described perfectly reproducible engineered catalyst constitutes a model system, which produces measurable amounts of product with our standard setup and thus allows for qualitative and quantitative conclusions. Figure 5 shows the product yields for both planar

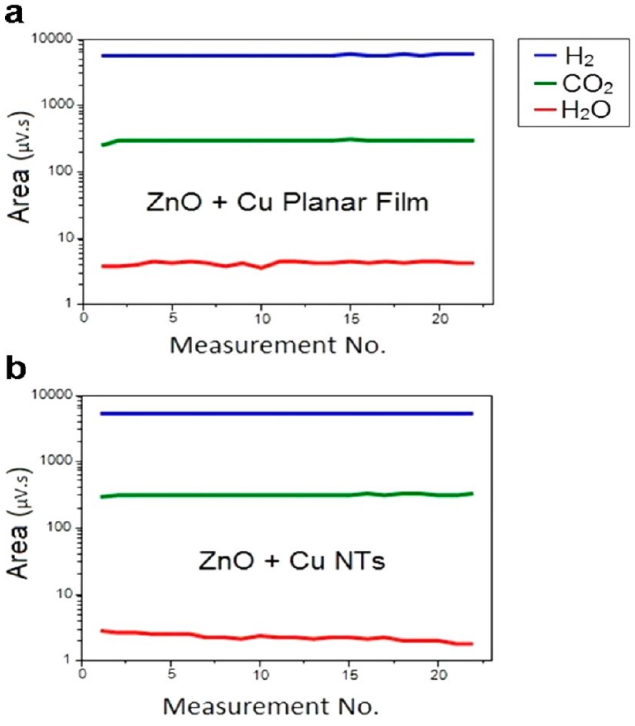

Figure 5. Reaction product yields in the presence of (a) the planar Cu/ZnO catalyst system and (b) the Cu/ZnO nanotube catalyst system. The catalysts were tested at 220 and 240 °C (each step 6 h), pressures of 40 bar, and gas flows of 1600 N mL·h^{-1} (75 % H_2 and CO_2).

and nanotube catalyst systems obtained from integration of the conductance values measured with the thermal conductivity detector (TCD) over the precalibrated retention times for each species.

Interestingly, although the planar system performed slightly better, both of the systems produced only trace amounts of methanol but ample amounts of water (see SI Figure S4 for gas chromatograms). As we failed to detect any CH_4 as one of the reaction products, we concluded that the water signal originated from the reverse water−gas shift reaction (RWGSR). Equation 3 shows the equation for RWGSR.

$$CO_2 + H_2 \rightleftharpoons CO + H_2O \quad \Delta H_{298K} = 9.84 \text{ kcal/mol} \tag{3}$$

The presence of water during the catalysis reaction indicates that the constructed catalysts were indeed active and were able to activate CO_2. The endothermic RWGSR is more favorable at high temperatures, as is visible in Figure 5a. The small step at measurement number 12 indicates a higher water content. Commonly, with the higher temperature the reactants themselves get further activated. Therefore, a small methanol signal was detected for the planar surface at 240 °C (see SI Figure S4). The planar sample produced 25% more water and at least detectable amounts of methanol. These results were contrary to what was expected since the NT sample had about ∼36-fold higher surface area. The planar sample had a total surface area of 40 mm^2, whereas the NT sample had 1420 mm^2 assuming a uniform NT diameter of 500 nm and length of 5 μm. Despite the fact that the NT sample had a higher ZnO surface area, our analysis showed that it contained less Cu. This is caused by the method of deposition for Cu. Thermal evaporation can work reasonably well for the deposition of thicker films on vertical structures, but it performed poorly for the ∼5 nm film on our HAR NTs. Ideally, a conformal Cu deposition process based on ALD would solve this problem and distribute Cu uniformly over the entire sample. However, the ALD Cu process is not very common.

Considering the calculated mass of the active species, the water yield is remarkable. By extrapolation of the water yield for the engineered catalysts to the weight of conventional catalyst used in our system (∼1000 mg), the model system shows a much higher activity (factor 70!) in RWGSR. Interestingly, even though our samples had the fraction of the surface area of the commercial catalyst, this high activation value indicates that high surface area alone does not guarantee better performance.

On another note, low selectivity to methanol over water is attributed to the high surface mobility of the Cu particles and their eventual aggregation into larger particles as seen in Figure 3. When the particles are mobile, intermediate species that form on the Cu particles such as HCOO, HCOOH, H_2COOH, HCO, H_2CO, and H_3CO cannot reside on the constantly evolving Cu surface facets to get ultimately upconverted to CH_3OH. Though it is not completely eliminated, this effect should be suppressed in the porous aggregates that are produced by the coprecipitation method where Cu particles are structurally trapped in the porous media. Therefore, finding methods to reduce Cu mobility could increase the performance of the industrial Cu/ZnO catalysts as well as the system studied here. Furthermore, the amount of water produced by the NT sample slowly decreased over the course of the reaction. This may have been caused by the mobile Cu species moving downward to the inner parts of the NTs, prolonging the diffusion times for the reactants and products inside the HAR nanostructures. Once again, it appears that producing catalysts with a high surface area alone does not bring an added advantage in terms of the conversion efficiency and system performance. This is in agreement with independent observations on classical and fluorinated Cu/ZnO/ZrO_2 catalyst systems produced by coprecipitation methods [Elias Frei, Ingo Krossing, to be published]. Diffusion characteristics of the reaction gasses need to be considered to improve overall conversion efficiency.

In summary, we have demonstrated a new technique for the fabrication of vertically oriented, high aspect ratio nanotubes and nanowires on Si. The proposed method was based on patterning with near-field phase shift lithography, deep trench etching with the Bosch process, and coating of the trenches

with atomic layer deposition. We produced ZnO and Al_2O_3 nanotubes to demonstrate the capability of the reported method.

Engineered Cu/ZnO planar and nanotube samples were prepared to study thermocatalytic methanol synthesis comparatively, and the following conclusions were made:

- Clear product signals for the engineered model systems with a minimal catalyst loading of 0.01 to 0.1 mg are encouraging and suggest a very active model system that should be studied in more detail in future work in a designated setup.
- Prepared samples showed 70 times higher CO_2 activation than the commercial catalysts.
- Although the nanotube sample has a higher surface area, it exhibited an inferior catalytic performance due to the lower amounts of Cu deposited.
- The method of deposition is very critical for improved catalyst distribution.
- Poor catalytic conversions of both systems were attributed to mobile Cu particles on the surface and accelerated nanocatalyst aging. Mobile Cu particles with unstable and constantly evolving surface facets possibly did not allow intermediate reaction species to stay on the catalyst surface for complete hydrogenation to CH_3OH.
- For increased catalytic performance, Cu mobility and catalyst aging need to be reduced, and the catalyst surface needs to be stabilized, for instance, by providing structural confinement, addition of impurities, or decreasing the process temperature.
- High aspect ratio structures such as pores or tubes with large surface areas may not improve catalytic conversion efficiency, and they need to be optimized with diffusion lengths of the reaction gasses in mind.

Overall, we demonstrated that engineered surfaces can be a valuable tool for mechanism exploration and process optimization for catalyst systems. However, more research is required to improve design and fabrication of such systems.

METHODS AND MATERIALS

Near-Field Phase Shift Lithography. Wafer-scale periodic hole patterns were generated by double exposing the AZ 5214 E type photoresist film through a fully transparent phase shift mask with a 90° rotation. Reversal bake and flood exposure were performed at 115 °C for 120 and 20 s, respectively, after which the wafer was submerged into AZ MIF 726 for development.

Reactive Ion Etching. The photoresist pattern was transferred to the thermal oxide layer by plasma etching with a gas mixture of CHF_3 (35 sccm)/CF_4 (15 sccm)/Ar (50 sccm) at 350 W.

Photoresist and Thermal SiO_2 Removal. Etched Si wafer was subjected to O_2 at 220 °C with a plasma power of 400 W after which the Si substrate was dipped into a 5% HF solution to remove the thermal oxide from the Si wafer.

Deep Reactive Ion Etching with Bosch Process. High aspect ratio Si trenches were etched in an ICP-type dry etcher manufactured by STS. For the passivation step, C_4F_8 (85 sccm) and for etching SF_6 (85 sccm) and O_2 (9 sccm) gasses were used with a coil power of 600 W. The platen generator was only used during the etch step and was set to 25 W. Under these conditions, an aspect ratio of 10 was achieved with a CD loss of 80 nm due to scalloping.

Atomic Layer Deposition. Si wafers with the etched trenches were coated by ZnO and Al_2O_3 using diethylzinc (DEZ)/water and trimethylaluminum (TMA)/water precursors, respectively, at 150 °C in a vertical flow-type hot wall reactor (OpAL; manufactured by Oxford Instruments). Before deposition, the reactor was pumped to 20 mTorr and maintained around 170−190 mTorr during the process. N_2 was used as the carrier and purge gas to deliver the reactants into the reactor and to remove the byproducts to prevent secondary CVD reactions in the reaction environment. The coating thickness was controlled by the number of deposition cycles in the process. The ZnO growth rate was approx. 0.2 nm/cycle, whereas Al_2O_3 was 0.1 nm/cycle at a deposition temperature of 150 °C.

Scanning Electron Microscopy. All samples were observed with a high-resolution SEM (Nova NanoSEM) manufactured by FEI with a nominal maximum resolution of 1 nm.

Transmission Electron Microscopy. All experiments were performed with a Zeiss LEO 912 type microscope at an acceleration voltage of 120 keV.

X-ray Reflectivity. A reflectometer from Philips equipped with two Goebel mirrors was employed for determining the layer thickness.

Rutherford Backscattering Spectroscopy. Measurements were performed with 1.4 MeV He^+ ions and a scattering angle of 170° with an UHV-high precision goniometer attached to the Jülich Tandetron accelerator.

Copper Deposition. 5 nm films were deposited in a thermal metal evaporator at 5×10^{-5} mbar with 99.99% pure Cu crucibles purchased from Kurt J. Lesker Company.

Catalysis Experiments. The nanoengineered surfaces were tested in a fixed-bed tube reactor coupled to a GC with a TCD detector. Each nanocatalyst was reduced prior to the measurement with H_2 and diluted with N_2 (4-100% hydrogen). The reactor was set under pressure (40 bar) and high temperature (220 and 240 °C) during the entire experiment. For methanol synthesis a gas mixture of H_2 (75%) and CO_2 (25%) was used (feed gas 1600 N mL h^{-1}). The reaction conditions were kept constant for 12 h.

ASSOCIATED CONTENT

Supporting Information

A schematic displaying the principle of the Bosch process, SEM images showing the profiles of high aspect ratio etched trenched under various processing conditions, water and methanol signals extracted from a gas chromatogram obtained during the catalysis experiments, and detailed information on the catalyst test station and the software. This material is available free of charge via the Internet at http://pubs.acs.org.

AUTHOR INFORMATION

Corresponding Authors

*E-mail: gueder@imtek.com.
*E-mail: elias.frei@ac.uni-freiburg.de.

Present Address

⊥Semikron s.r.o., Steruska ul. 3, 92203, Vrbove, Slovakia (R.L.).

Notes

The authors declare no competing financial interest.

ACKNOWLEDGMENTS

We would like to thank Prof. Dr. Yang Yang for the fruitful discussions and the University of Freiburg, the German Research Foundation, as well as the Deutsche Bundesstiftung Umwelt DBU for financial support (under contract: ZA 191/24-1; DBU-project MethaKats).

REFERENCES

(1) Xia, Y.; Yang, P.; Sun, Y.; Wu, Y.; Mayers, B.; Gates, B.; Yin, Y.; Kim, F.; Yan, H. *Adv. Mater.* **2003**, *15*, 353−389.
(2) Yan, H.; Choe, H. S.; Nam, S.; Hu, Y.; Das, S.; Klemic, J. F.; Ellenbogen, J. C.; Lieber, C. M. *Nature* **2011**, *470*, 240−244.
(3) Wang, G.; Wang, H.; Ling, Y.; Tang, Y.; Yang, X.; Fitzmorris, R. C.; Wang, C.; Zhang, J. Z.; Li, Y. *Nano Lett.* **2011**, *11*, 3026−3033.
(4) Zhang, Y.; Su, L.; Manuzzi, D.; de los Monteros, H. V. E.; Jia, W.; Huo, D.; Hou, C.; Lei, Y. *Biosens. Bioelectron.* **2012**, *31*, 426−432.

(5) Menzel, A.; Guebeli, R.; Güder, F.; Weber, W.; Zacharias, M. *Lab Chip* **2013**, *13*, 4173−4179.
(6) Büttner, C.; Zacharias, M. *Appl. Phys. Lett.* **2012**, *89*, 263106−263106.
(7) Güder, F.; Yang, Y.; Goetze, S.; Berger, A.; Ramgir, N.; Hesse, D.; Zacharias, M. *Small* **2012**, *6*, 1603−1607.
(8) Hoffmann, S.; Östlund, F.; Michler, J.; Fan, H.; Zacharias, M.; Christiansen, S.; Ballif, C. *Nanotechnology* **2007**, *18*, 205503.
(9) Subannajui, K.; Güder, F.; Zacharias, M. *Nano Lett.* **2010**, *11*, 3513−3518.
(10) Bjork, M.; Hayden, O.; Schmid, H.; Riel, H.; Riess, W. *Appl. Phys. Lett.* **2007**, *90*, 142110−142110.
(11) Vila, L.; Vincent, P.; Dauginet-De Pra, L.; Pirio, G.; Minoux, E.; Gangloff, L.; Demoustier-Champagne, S.; Sarazin, N.; Ferain, E.; Legras, R.; Piraux, L.; Legagneux, P. *Nano Lett.* **2004**, *4*, 521−524.
(12) Subannajui, K.; Güder, F.; Danhof, J.; Menzel, A.; Yang, Y.; Kirste, L.; Wang, C.; Cimalla, V.; Schwarz, U.; Zacharias, M. *Nanotechnology* **2012**, *23*, 235607.
(13) www.epa.gov/climatechange/ghgemissions/usinventoryreport.html, "Inventory of U.S. Greenhouse gas emissions and sinks: 1990−2011", United States Environmental Protection Agency, 2013.
(14) Saito, M. *Catal. Surv. Asia* **1998**, *2*, 175−184.
(15) Zander, S.; Kunkes, E. L.; Schuster, M. E.; Schumann, J.; Weinberg, G.; Teschner, D.; Jacobsen, N.; Schloegl, R.; Behrens, M. *Angew. Chem., Int. Ed.* **2013**, *52*, 6536−6540.
(16) Behrens, M.; Studt, F.; Kasatkin, I.; Kühl, S.; Haevecker, M.; Abild-Pedersen, F.; Zander, S.; Girgsdies, F.; Kurr, P.; Kniep, B.L.; Tovar, M.; Fischer, R.W.; Norskov, J. K.; Schloegl, R. *Science* **2012**, *336*, 893−897.
(17) Behrens, M.; Zander, S.; Kurr, P.; Jacobsen, N.; Senker, J.; Koch, G.; Ressler, T.; Fischer, R. W.; Schloegl, R. *J. Am. Chem. Soc.* **2013**, *135*, 6061−6068.
(18) Güder, F.; Yang, Y.; Krüger, M.; Stevens, G. B.; Zacharias, M. *ACS Appl. Mater. Interfaces* **2010**, *2*, 3473−3478.
(19) Güder, F.; Yang, Y.; Kücükbayrak, U. M.; Zacharias, M. *ACS Nano* **2013**, *7*, 1583−1590.
(20) Knez, M.; Nielsch, K.; Niinistμ, L. *Adv. Mater.* **2007**, *19*, 3425−3438.
(21) George, S. M. *Chem. Rev.* **2009**, *110*, 111−131.
(22) Elam, J.; Routkevitch, D.; Mardilovich, P.; George, S. *Chem. Mater.* **2003**, *15*, 3507−3517.
(23) Bachmann, J.; Jing, J.; Knez, M.; Barth, S.; Shen, H.; Mathur, S.; Goesele, U.; Nielsch, K. *J. Am. Chem. Soc.* **2007**, *129*, 9554.
(24) Banerjee, P.; Perez, I.; Henn-Lecordier, L.; Lee, S. B.; Rubloff, G. W. *Nat. Nanotechnol.* **2009**, *4*, 292−296.
(25) Gu, D.; Baumgart, H.; Abdel-Fattah, T. M.; Namkoong, G. *ACS Nano* **2010**, *4*, 753−758.
(26) Holländer, B.; Heer, H.; Wagener, M.; Halling, H.; Mantl, S. *Nucl. Instrum. Methods, B* **2000**, *161*, 227−230.